ACS APPLIED MATERIALS & INTERFACES

www.acsami.org
Research Article

Permeation Barriers Grown by Atomic Layer Deposition Endow Non-Fullerene Organic Solar Cells with Damp-Heat Resilience

Florian Zimmermann, Pang Wang, Christian Tückmantel, Timo Maschwitz, Ralf Heiderhoff, Kai Oliver Brinkmann,* and Thomas Riedl*

Cite This: ACS Appl. Mater. Interfaces 2025, 17, 30924−30931
Read Online

ACCESS | Metrics & More | Article Recommendations | Supporting Information

ABSTRACT: Organic solar cells (OSCs) based on nonfullerene acceptors have seen tremendous progress recently, which qualifies them as a serious next-generation photovoltaic technology. However, their long-term stability is still a key issue that needs to be addressed on the way to commercialization. For relevant long-term stability, gas diffusion barriers are needed to protect the OSCs against ambient gases such as oxygen and moisture. Here, we explore gas diffusion barriers grown by atomic layer deposition (ALD) and demonstrate that aluminum oxide barriers grown at 80 °C afford OSCs that can be operated in the maximum power point in ambient air for more than 1000 h without notable degradation. At the same time, we show that under damp heat conditions, i.e., elevated temperature and humidity, better barriers are needed, that require growth temperatures of >80 °C, which are not tolerated by our standard *p-i-n* type OSCs. We significantly improve the thermal stability of our OSCs by the introduction of aluminum-doped zinc oxide nanoparticles (AZO-NPs) as electron extraction layers. OSCs using AZO-NPs are shown to withstand the ALD growth of barrier layers up to 120 °C. Finally, by introducing an aluminum oxide/titanium oxide multilayer barrier, we successfully prevent the corrosion of neat aluminum oxide under damp heat conditions, and OSCs encapsulated with these nanolaminates retain above 80% of their initial efficiency after 1000 h at 70 °C/70% relative humidity. Our results contribute to the improved stability of NFA OSCs even in harsh environments.

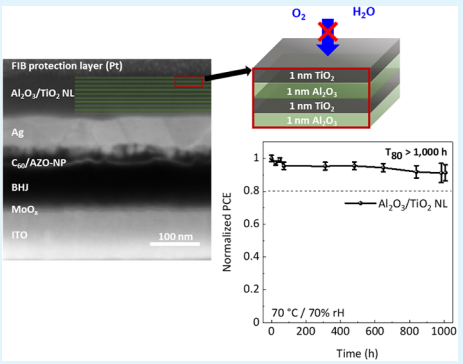

KEYWORDS: *organic solar cells, atomic layer deposition, gas diffusion barrier, thermal stability, nonfullerene acceptor*

INTRODUCTION

Organic solar cells (OSCs) offer distinct benefits such as low-cost solution processing, a low carbon footprint, lightweight design, mechanical flexibility, and scalability for large-area production.[1−5] These characteristics enable significant potential for OSCs in a wide array of innovative applications, such as portable devices and the Internet of Things (IoT), where traditional silicon (Si) solar cells face limitations.[6−9] A breakthrough in the field of OSCs was achieved with the introduction of Y-family nonfullerene acceptors (NFAs),[10] which unlocked efficiencies of up to 20%.[11,12] Despite this notable progress, the stability of OSCs upon illumination and exposure to elevated temperatures/humidity levels remains a key challenge.[1] The long-term stability of NFA OSCs is influenced by several factors, including material stability, morphological stability of the bulk heterojunction (BHJ), and interface stability, e.g., photocatalytic processes at the NFA/ZnO interface.[13]

Some strategies have been developed to address the aforementioned stability challenges. For example, the polymerization of NFAs significantly enhances thermal stability while maintaining relatively high efficiency.[14] The incorporation of fullerenes as a third component in so-called ternary cells has been found to mitigate thermally driven morphology degradation of the BHJ.[15−17] Moreover, the photocatalytic degradation of the NFA when in contact with a ZnO-based electron extraction layer (EEL) in inverted OSCs can be avoided by the introduction of a protective interlayer or by replacing ZnO with SnO_2.[18−20]

Notwithstanding the aforementioned measures, OSCs still require effective protection when exposed to ambient air. For example, the donor polymer PM6, which is frequently used in combination with a wide variety of acceptors, exhibits some notable twisting of its backbone upon illumination, which is facilitated by the presence of air.[21] Additionally, the cyano groups of Y6 exhibit instability in the presence of water, and illumination accelerates this degradation process.[22] At the same time, oxygen exposure is known to be critical, as ultraviolet (UV)-light-triggered photooxidation causes damage in OSCs.[20,23]

Received: February 25, 2025
Revised: April 18, 2025
Accepted: April 21, 2025
Published: May 15, 2025

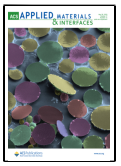

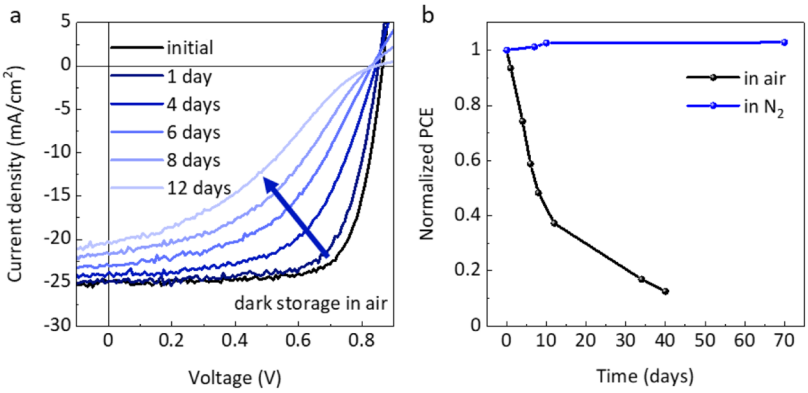

Figure 1. a) J/V characteristics of the OSC before and after dark storage in air. b) Normalized PCE over time of the OSC stored in darkness in air compared to an OSC stored in nitrogen (N_2).

As such, concepts to suppress the ingress of oxygen and moisture into the solar cells are mandatory.[24] Traditional glass-lid encapsulation is very effective, but it may sacrifice some of the paradigms associated with OSCs, such as lightweight, low cost, and mechanical flexibility.[24−27] On the contrary, thin-film gas diffusion barriers (GDBs) offer an attractive alternative. A typical figure of merit for GDBs is their water vapor transmittance rate (WVTR), which specifies how much water (in grams) can penetrate a square meter of the barrier in 1 day. Typical values for the WVTR of a barrier in order to qualify for encapsulation of organic electronic devices are in the range of 10^{-4}−10^{-6} g/(m^2 day).[28] Among the deposition techniques used to prepare layers with a WVTR in this range, atomic layer deposition (ALD) stands out, as it allows for the preparation of dense, conformal layers at low temperatures, which is a critical requirement if the barrier is to be deposited on top of the OSC. GDBs grown by ALD have been shown to reach WVTRs in the order of 10^{-6} g/(m^2 day), and they have been successfully used in organic light-emitting diodes (OLEDs).[29−33] A study that explores the applicability of ALD-grown GDBs to encapsulate high-performance NFA OSCs is missing as of yet.

Here, we show the outstanding potential of thin-film GDBs grown by ALD to overcome the instability of NFA OSCs in ambient air. Specifically, we demonstrate that an aluminum oxide (Al_2O_3) GDB grown at 80 °C affords devices that can be operated in the maximum power point (MPP) in air for more than 1000 h without notable degradation. The situation changes, however, under damp heat conditions (70 °C/70% relative humidity (rH)), where severe degradation of the encapsulated cells manifests, even upon storage. Consequently, an improved encapsulation layer is needed, which is typically achieved through higher deposition temperatures. In the present device architecture, we show that the thermal instability of the bathocuproine (BCP) electron extraction layer (EEL) restricts the maximum growth temperature the cell can tolerate to ≤80 °C. To overcome this limit, we introduce aluminum-doped zinc oxide nanoparticles (AZO-NPs) as the EEL with superior thermal stability, allowing for the growth of improved GDBs at temperatures up to 120 °C. Over several hundred hours under damp heat conditions, corrosion of Al_2O_3 leads to degradation of the barrier layer. Therefore, we introduced an ALD-grown nanolaminate (NL) consisting of Al_2O_3 and titanium oxide (TiO_2) multilayers. We evidence that this NL barrier effectively withstands high humidity without corrosion and affords solar cells that retain above 80% of their initial efficiency even after more than 1000 h under damp heat conditions (70 °C/70% rH). We foresee that our work will pave the way toward improved stability of NFA OSCs even in harsh environments.

RESULTS AND DISCUSSION

For the OSCs in this study, we selected a ternary blend consisting of PM6:Y6:$PC_{61}BM$ (ratio 1:1.2:0.2) as an absorber layer in a p-i-n device architecture ITO/MoO_x/PM6:Y6:$PC_{61}BM$/C_{60}/BCP/Ag. These cells have already shown excellent reproducibility and high power conversion efficiencies (PCEs) in our previous work.[34,35] Further details on the solar cell fabrication process are provided in the Experimental Section. The typical characteristics of the devices studied in this paper are: PCE = 16.4 ± 0.2%, fill factor (FF) = 74 ± 0.7%, open-circuit voltage (V_{OC}) = 0.86 ± 0.01 V, and short-circuit current density (J_{SC}) = 25.7 ± 0.4 mA/cm^2 (Table S1). Detailed current density versus voltage (J/V) statistics are presented in Figure S1.

To investigate the long-term stability of our NFA OSCs when exposed to air, we initially studied their "shelf lifetime" in the dark without encapsulation. As shown in Figure 1a,b, we observed a significant decrease in the FF, resulting in a reduction in the overall PCE (<80% of the initial value) within the first 4 days of storage. Detailed J/V characteristics of the device upon aging are provided in Table S2. In contrast, the same kind of devices remained unchanged when stored under inert conditions (N_2) for more than 70 days (Figure 1b).

In previous studies, the PM6:Y6 system showed notable instability upon illumination in air.[36] Raman spectroscopy of neat PM6 films was used to unravel the root cause of the degradation mechanism, which was attributed to the illumination-induced dihedral twist between the benzodithiophene (BDT) and backbone thiophene units of PM6. This twisting of the backbone was found to be accelerated in the presence of ambient air.[21] Our own Raman spectroscopy study of neat PM6 layers aged in a controlled humid environment (only H_2O but no O_2) is in line with these previous findings (Figure S2b). While under inert conditions, the Raman signal of the PM6 remained unaltered after 24 h of continuous illumination (λ = 617 nm, P = 160 mW/cm^2) (Figure S2a), the same layer showed a clear sign of backbone twisting already after 1 h in the presence of H_2O molecules (Figure S2b). The twisting of the backbone was previously found to result in the formation of polaron pairs that give rise to trap-mediated recombination and result in the degradation of device

https://doi.org/10.1021/acsami.5c03977
ACS Appl. Mater. Interfaces 2025, 17, 30924−30931

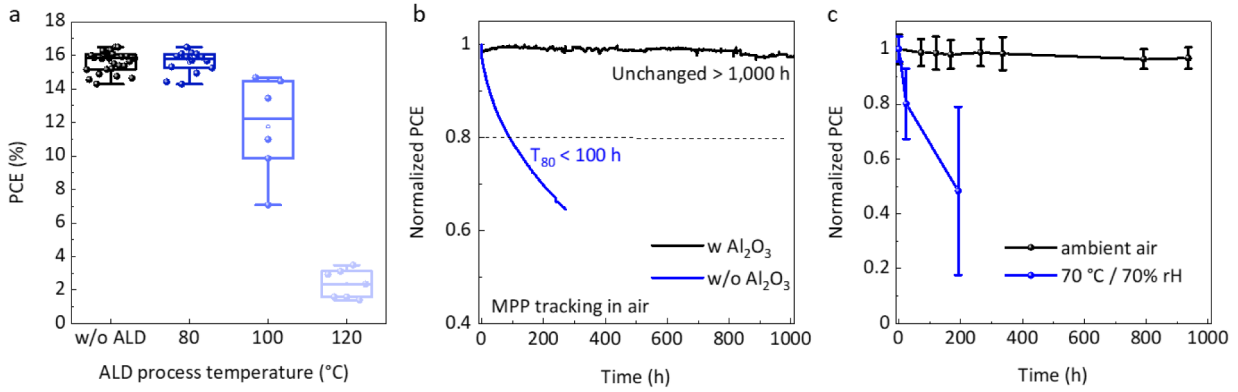

Figure 2. a) PCE of encapsulated OSCs versus ALD process temperature of the Al_2O_3 GDB. b) Normalized PCE of the OSCs versus time with and without (w/o) Al_2O_3 GDB in air illuminated with a 617 nm LED and operated at the maximum power point. c) Normalized PCE of the OSCs with Al_2O_3 GDB versus time upon storage in ambient air compared to storage inside a climate cabinet at 70 °C/70% rH (both without illumination).

performance. In contrast, no significant changes of the Raman spectra of Y6 upon illumination (617 nm LED) under inert N_2 and humid N_2 conditions were found (Figure S2c,d). Nevertheless, our findings combinedly underscore the need for an effective barrier to shield the sensitive organic materials from air exposure.

As outlined above, ALD-grown thin-film GDBs are promising avenues for the encapsulation of organic electronic devices. To explore the applicability of ALD-grown Al_2O_3 barrier layers, 100 nm thick Al_2O_3 layers were deposited on top of our OSCs using trimethylaluminum (TMA) and water (H_2O) as precursors. Al_2O_3 is chosen as a starting material because it provides a very robust low-temperature ALD process[37] and the precursor TMA is available in large quantities at relatively low cost, which is promising with respect to upscaling. Note that the fresh OSCs were transferred to the ALD reactor without an inert break immediately after the deposition of the silver top electrode. Details of the ALD process can be found in the Experimental Section. Previous reports have shown that the WVTR of ALD-grown GDBs depends on the deposition temperature, with a continuous improvement (lowered WVTR) found when going from 80 to 150 °C.[32]

As such, our first study explored the impact of the ALD growth temperature on the characteristics of our cells. While the devices encapsulated at 80 °C remained unaltered, the cells at higher ALD temperatures (≥100 °C) already showed notable signs of deterioration (Figure 2a). At 100 °C, predominantly the FF degraded, while at 120 °C, all device characteristics indicated severe damage (Figure S3). We discuss the root cause of this degradation in more detail below. For the moment, to ensure the deposition of the GDB without damaging the device, an ALD process temperature of 80 °C was selected. Next, the long-term stability of the devices was tested in air under continuous illumination (one sun equivalent) in the MPP. To exclude photoinduced degradation, which might even take place under inert conditions, a LED emitting at 617 nm was used as the illumination source for this experiment, which has been reported to have no adverse effect on the photostability of PM6:Y6 OSCs.[38−40] As shown in Figure 2b, the Al_2O_3 GDB endowed the OSCs with exceptional long-term stability in ambient air. The cells maintained their performance for more than 1000 h of continuous operation in the maximum power point (MPP) without a sign of deterioration, while the cells without GDB exhibited significant degradation already within the first 100 h. Encouraged by this impressive finding, we explored more stressful ambient conditions. Specifically, we subjected the cells to a damp heat atmosphere in a climate cabinet with an elevated temperature and high relative humidity (70 °C/70% rH). Strikingly, the encapsulated cells that proved outstandingly stable in our lab atmosphere (21 °C/55% rH) experienced rapid degradation at (70 °C/70% rH) (Figure 2c).

Following the discussion above, in order to improve the GDB barrier properties, we considered higher deposition temperatures (>80 °C) in the ALD process. To this end, we need to better understand the root cause of degradation inferred by elevated growth temperatures (Figure 2a). Therefore, we conducted annealing studies on our OSCs by placing them on a hot plate inside an inert glovebox for 2 h. As shown in Figure 3a, OSCs subjected to annealing temperatures above 80 °C show a deterioration in their cell characteristics, in agreement with our findings shown in Figure 2a.

Very surprisingly, if only a partial stack of the device (i.e., ITO/MoO_x/BHJ without the EEL and without the top electrode, "half cell") was annealed and the C60/BCP/Ag layers were deposited afterward, no degradation was found even for an annealing temperature of up to 120 °C (Figure 3b). These findings suggest that the electron extraction layers (C_{60}/BCP) and/or the Ag top electrode limit the thermal stability of the OSCs. In previous studies, a strong tendency of BCP toward crystallization at elevated temperatures has been found, giving us a hint that BCP might be the weak link in our OSCs at elevated temepratures.[41] In an aim to overcome this issue, we exploit the insights of our previous work on perovskite solar cells, in which solution-processed AZO-NP electron extraction layers showed promising resilience against elevated temperatures.[34,42] In analogy, a beneficial impact on the thermal stability of OSCs has been achieved by using ZnO-NPs.[43] In our revised OSCs, we therefore replaced the BCP layer with AZO-NPs. Very encouragingly, the resulting OSCs incorporating a bilayer of C_{60} and AZO-NPs exhibited high FFs and a comparable V_{OC} to the reference device with a C_{60}-BCP EEL (Figure 3c). It is important to note that the somewhat lower current density found in the AZO devices is likely due to optical effects. To understand this effect better, we used an optical simulation (SETFOS), where we modeled the dependence of the J_{SC} on the thickness of the BCP or AZO layer, respectively (Figure S4c). As a general trend, J_{sc} decays with increasing EEL thickness (regardless of whether BCP or

https://doi.org/10.1021/acsami.5c03977
ACS Appl. Mater. Interfaces 2025, 17, 30924−30931

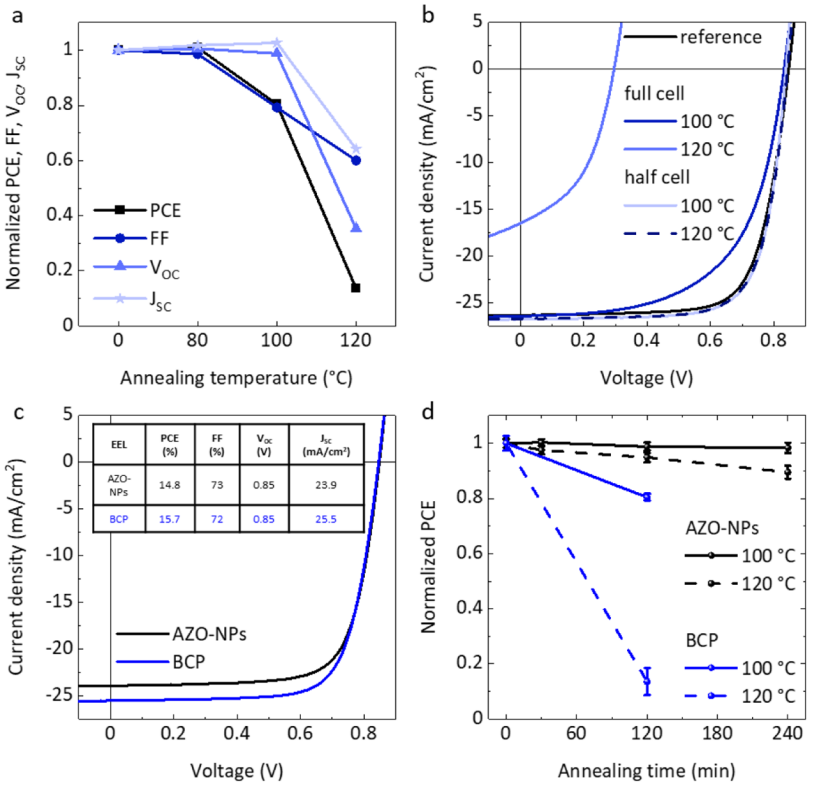

EEL	PCE (%)	FF (%)	V_{OC} (V)	J_{SC} (mA/cm²)
AZO-NPs	14.8	73	0.85	23.9
BCP	15.7	72	0.85	25.5

Figure 3. a) Normalized *J*/*V* characteristics versus annealing temperature. b) *J*/*V* characteristics of OSCs, with annealing of the half or full cell. c) *J*/*V* characteristics comparison between OSCs with AZO-NPs and the BCP EEL. d) Normalized PCE versus annealing time of the OSCs using either AZO-NPs or the BCP EEL.

AZO is used). In the case of the AZO-NPs, their size of around 12 nm limits the minimum layer thickness, while the thickness of the thermally evaporated BCP layer is typically chosen as 5 nm. We want to note, however, that while we do not expect this to be a fundamental issue, an optimization of the optical design of the device structure is beyond the scope of this work.

In any event, replacing the BCP EEL with AZO-NPs afforded OSCs with substantially improved thermal stability and resilience against thermal treatment (Figure 3d). Consequently, we are now able to grow our Al_2O_3 GDBs even at 120 °C without damaging the OSCs, which immediately results in a significantly improved shelf life under damp heat conditions (70 °C/70% rH), and the corresponding OSCs showed a T_{80} of greater than 600 h (Figure 4b), which is significantly higher than the T_{80} of only 16 h in devices with a GDB grown at 80 °C. Notwithstanding the obvious improvement brought by the Al_2O_3 GDBs grown at 120 °C, after roughly 650 h, the solar cells experienced increasingly rapid degradation.

To understand this behavior, it is important to consider that ALD-grown Al_2O_3 layers are susceptible to corrosion when exposed to damp heat conditions, which results in the formation of Al−OH species in the layers.[31,44] This corrosion effect was found to severely compromise the barrier properties of the Al_2O_3 films.[30,31] As concepts to mitigate the corrosion of Al_2O_3, multilayers (so-called nanolaminates), e.g., Al_2O_3 and SiO_2[44] or Al_2O_3 and ZrO_2[30], can be considered. It has to be kept in mind that the deposition process of the second material needs to be compatible with the temperature constraints imposed by the OSC. As such, we selected to explore nanolaminates of Al_2O_3 and TiO_2. TiO_2 is known to be more resilient against water exposure, but previous work using

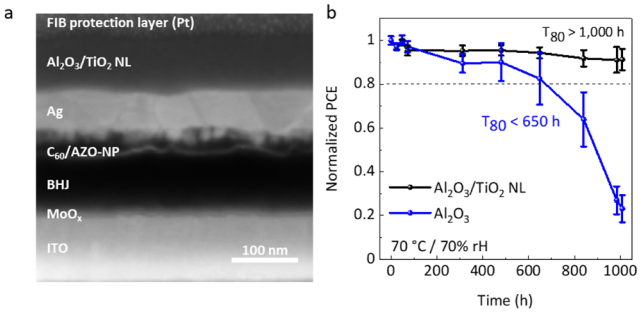

Figure 4. a) Scanning electron microscopy (SEM) cross-section visualizing the layer sequence of the OSC with optimized AZO-NP EEL and an Al_2O_3/TiO_2 nanolaminate (NL) GDB grown at 120 °C ALD reactor temperature. b) Normalized PCE versus time of OSCs with an Al_2O_3 or an Al_2O_3/TiO_2 NL GDB under dark storage in a climatic chamber at 70 °C/70% rH.

calcium tests has revealed that neat TiO_2 layers contain pinholes that originated from a limited wettability of the ALD-grown TiO_2 on top of metals.[33,45] These pinholes provided permeation paths for moisture and oxygen and overall rendered neat TiO_2 of limited use as a barrier.[33,46] It has been shown that the Al_2O_3 sublayers guaranteed excellent wetting of the other metal oxide (ZrO_2 or TiO_2) and prevented crystallization and the formation of pinholes.[31,33,46] The Al_2O_3/TiO_2 barriers can be grown by ALD at similarly low temperatures using $TiCl_4$ and H_2O as precursors for TiO_2,[33] and they have shown a WVTR in the range of 8×10^{-5} g/(m² day) at (70 °C/70% rH). We stress that these Al_2O_3/TiO_2 laminates have not been studied in the context of OSCs before. The device architecture using the Al_2O_3/TiO_2

https://doi.org/10.1021/acsami.5c03977
ACS Appl. Mater. Interfaces 2025, 17, 30924−30931

nanolaminate as an encapsulation layer is shown in Figure 4a. Note that, as the sublayer thickness of the Al_2O_3 and TiO_2 layers is only 1 nm, the sublayers cannot be resolved in the SEM cross-section. The thickness of the nanolaminate is about 100 nm (see also Figure S5).

As a striking improvement, the efficiency of our NFA OSCs encapsulated by these Al_2O_3/TiO_2 nanolaminates (sublayer thicknesses: Al_2O_3: 1 nm, TiO_2: 1 nm) with an overall thickness of 100 nm grown at 120 °C remained above 80% of its initial efficiency even after more than 1000 h under damp heat conditions (70 °C/70% rH) (Figure 4b). In a previous study, we investigated the impact of the nanolaminate layer thickness on the prevalence of pinhole defects by encapsulating Ca pads that were then subjected to damp heat conditions. We found a significantly reduced failure probability when increasing the thickness from 50 to 100 nm.[33] Toward thicker layers >300 nm, the tensile strain in the ALD-grown layers caused the formation of cracks. As such, the 100 nm barrier thickness in this work is a reasonable choice.

Please note that while our Al_2O_3/TiO_2 nanolaminate barriers provide an important building block to protect OSCs against ambient gases (e.g., moisture), the photostability of the organic active materials and the adjacent charge transport layers needs further attention, as outlined in the Introduction section. In single junctions, adding filters, that block harmful spectral components, has been discussed,[47] while in tandem architectures, the wide-gap subcell may act as an inherent spectral filter, providing operational stability for the organic subcell.[34,40]

As a final remark, ALD is originally a batch-processing technique that is operated under vacuum conditions. Therefore, the suitability of ALD for high-throughput, low-cost, and roll-to-roll manufacturing is sometimes questioned. However, there are several concepts to speed up ALD.[48] Among them, spatial ALD (S-ALD) can be operated continuously even at atmospheric pressure and provides an avenue for roll-to-roll ALD processing.[49,50]

CONCLUSIONS

In this study, we were able to overcome the instability of nonfullerene organic solar cells (NFA OSCs) in ambient air by introducing thin-film gas diffusion barriers grown by low-temperature atomic layer deposition (ALD). Specifically, we demonstrated that Al_2O_3 barriers grown at 80 °C allowed the encapsulated OSCs to withstand more than 1000 h of continuous operation in air without any signs of degradation. However, elevated temperature and humidity levels showed the need for further improved barrier layers that required ALD growth temperatures of >80 °C, which could not be tolerated by standard *p-i-n* type OSCs. We could associate the thermal instability with the bathocuproine (BCP) electron extraction layer used in our standard devices. A significant improvement of the OSCs against thermal stress was achieved by the introduction of aluminum-doped zinc oxide nanoparticles as electron extraction layers, which allowed the OSCs to withstand the ALD growth of barrier layers even up to 120 °C. While neat Al_2O_3 layers corroded at elevated temperature and humidity levels, which limits their applicability under these conditions, we demonstrated that Al_2O_3/TiO_2 multilayers are significantly more robust. OSCs encapsulated with these Al_2O_3/TiO_2 nanolaminates retained above 80% of their initial efficiency even after 1000 h under damp heat conditions (70 °C/70% relative humidity). Our findings present a promising approach for improving the air stability of next-generation solar cells, further advancing their potential for commercialization.

EXPERIMENTAL SECTION

Materials Synthesis and Device Fabrication. *Organic Solar Cells.* OSCs were built in the p-i-n device architecture. All processing steps were carried out either under an inert atmosphere or high vacuum without inert breaks. As the substrate, we used indium tin oxide (ITO)-coated glass (17 × 17 mm^2) with a photoresist patterned to define an active area of 3.14 mm^2. As hole extraction layer (HEL) 15 nm of molybdenum oxide (MoO_x) was thermally evaporated in a high vacuum (10^{-7} mbar) on top of the ITO bottom electrode. For the photoactive system, PM6:Y6:$PC_{61}BM$ (PM6 and Y6 from Solarmer Materials and $PC_{61}BM$ from American Dye Source) with a weight ratio of 1:1.2:0.2 were dissolved in chloroform (polymer concentration 7 mg mL^{-1}) and stirred for 3 h at 50 °C. 5 min before processing the BHJ, 0.5 vol % of 1-chloronaphthalene (Sigma-Aldrich) was added to the solution. Spin-coating was performed dynamically (solution was dropped onto the middle of the rotating substrate) at 2,500 rpm for 60 s. A subsequent thermal annealing step at 100 °C for 10 min was applied. For efficient electron extraction, a bilayer of 10 nm C_{60} and 5 nm BCP was thermally evaporated in a high vacuum (10^{-7} mbar), followed by 100 nm silver as an opaque top electrode. As an alternative to BCP, AZO layers were also used, processed from a nanoparticle (NP) dispersion (Avantama AG, N21x, 2.5 wt % in a mixture of alcohols) diluted with isopropanol (1:2) and spin-coated at 4000 rpm for 20 s using a ramp of 6 s. The AZO layers were subsequently annealed at 80 °C for 30 min.

Thin-Film Gas Diffusion Barriers. For the ALD deposition of the thin-film GDBs, the solar cells were transferred into a Beneq TFS-200 reactor (base pressure: 1.5 mbar) without an inert break. Al_2O_3 layers were grown from trimethylaluminum (TMA) and water (H_2O). The reactor temperature during the deposition was controlled within the range of 80−120 °C. The precursor was kept at room temperature. The optimized nanolaminate was grown at a reactor temperature of 120 °C from the precursors TMA for the preparation of Al_2O_3 and $TiCl_4$ for the preparation of TiO_2. The precursors were both kept at room temperature. As an oxidant, H_2O has been used. The Al_2O_3/TiO_2 nanolaminates were prepared by the sequential deposition of 9 cycles of (TMA, H_2O) and 15 cycles of ($TiCl_4$, H_2O), which results in respective sublayers of 1 nm of Al_2O_3 and 1 nm of TiO_2. Specifically, TMA, $TiCl_4$ and H_2O were pulsed for 150 ms, each followed by a 5-s N_2 purge. About 100 nm of the nanolaminate was grown by 50 alternate depositions of 1 nm Al_2O_3 and 1 nm TiO_2.

Materials and Device Characterization. *J/V Measurement.* *J/V* characteristics of solar cells were recorded outside the glovebox under a continuous flow of nitrogen by using a Keithley 2400 source measurement unit (SMU) and a 300 W Newport solar simulator (model 91160, AM1.5G, 100 mW cm^{-2}) calibrated with a certified IEC 60904−9-compliant Si reference cell (Rera Systems). *J/V* characteristics were recorded with a scanning speed of 500 mV s^{-1} under AM1.5 G illumination. Long-term measurements were conducted by continuous MPP tracking in air under the illumination of a 617 nm LED light source (Thorlabs M617L5). We set the intensity of the light source to generate a J_{SC} comparable to that of AM1.5G sunlight illumination.

Raman Measurement. Raman measurements were conducted using a confocal Raman system (MonoVista CRS+), with a 488 nm laser (for PM6) and a 633 nm laser (for Y6) as the excitation sources, and a 2400 L/mm grating (for PM6) or a 1200 L/mm grating (for Y6). To minimize laser-induced damage and to ensure an averaged signal across the sample, we continuously scanned the sample stage at a speed of approximately 5 mm/s. A custom sample holder was used to flush N_2 continuously, either dry or humidified. The humidified N_2 was generated by bubbling dry N_2 through water in a sealed metal container, which was then connected to the sample holder.

Scanning Electron Microscopy. The SEM cross-section image was obtained with an in-lens detector of Gemini 2 SEM (Zeiss Crossbeam 550) at an acceleration voltage of 5 kV at a working distance of 3.5

https://doi.org/10.1021/acsami.5c03977
ACS Appl. Mater. Interfaces 2025, 17, 30924−30931

mm and at a tilt of 36 ° (stage tilt 54 °). The cross-section was prepared by using focused ion beam (FIB) milling with a gallium (Ga) source. A protective layer of approximately 100 nm of platinum (Pt) was first deposited via electron beam (5 kV acceleration voltage, 14 nA beam current) depostion. A second Pt protection layer, about 1 μm thick, was then deposited using FIB (30 kV acceleration voltage and 300 pA beam current) on top of the initial thin Pt layer. Milling was performed with a beam current of 1.5 nA. Finally, the cross-sectional area was cleaned by using a beam current of 150 pA.

■ ASSOCIATED CONTENT

Supporting Information

The Supporting Information is available free of charge at https://pubs.acs.org/doi/10.1021/acsami.5c03977.

Additional *J*/*V* characteristics of the OSCs, Raman spectroscopy of PM6 and Y6, optical simulation of the device stack, SEM cross-section image, and stylus profilometer measurement of the NL (PDF)

■ AUTHOR INFORMATION

Corresponding Authors

Kai Oliver Brinkmann − *Institute of Electronic Devices, University of Wuppertal, Wuppertal 42119, Germany; Wuppertal Center for Smart Materials & Systems (CM@S), University of Wuppertal, Wuppertal 42119, Germany;* orcid.org/0000-0002-2124-3904; Email: brinkmann@uni-wuppertal.de

Thomas Riedl − *Institute of Electronic Devices, University of Wuppertal, Wuppertal 42119, Germany; Wuppertal Center for Smart Materials & Systems (CM@S), University of Wuppertal, Wuppertal 42119, Germany;* orcid.org/0000-0003-1084-316X; Email: t.riedl@uni-wuppertal.de

Authors

Florian Zimmermann − *Institute of Electronic Devices, University of Wuppertal, Wuppertal 42119, Germany; Wuppertal Center for Smart Materials & Systems (CM@S), University of Wuppertal, Wuppertal 42119, Germany*

Pang Wang − *Institute of Electronic Devices, University of Wuppertal, Wuppertal 42119, Germany; Wuppertal Center for Smart Materials & Systems (CM@S), University of Wuppertal, Wuppertal 42119, Germany;* orcid.org/0000-0002-9666-1422

Christian Tückmantel − *Institute of Electronic Devices, University of Wuppertal, Wuppertal 42119, Germany; Wuppertal Center for Smart Materials & Systems (CM@S), University of Wuppertal, Wuppertal 42119, Germany*

Timo Maschwitz − *Institute of Electronic Devices, University of Wuppertal, Wuppertal 42119, Germany; Wuppertal Center for Smart Materials & Systems (CM@S), University of Wuppertal, Wuppertal 42119, Germany*

Ralf Heiderhoff − *Institute of Electronic Devices, University of Wuppertal, Wuppertal 42119, Germany; Wuppertal Center for Smart Materials & Systems (CM@S), University of Wuppertal, Wuppertal 42119, Germany;* orcid.org/0000-0001-7615-4186

Complete contact information is available at: https://pubs.acs.org/10.1021/acsami.5c03977

Notes

The authors declare no competing financial interest.

■ ACKNOWLEDGMENTS

We acknowledge the Deutsche Forschungsgemeinschaft (DFG) (within the SPP 2196: grant numbers RI 1551/15-2, RI 1551/12-2, RI1551/22-1, and RI 1551/23-1) and the Bundesministerium für Bildung und Forschung (BMBF) (grant number 01DP20008) for financial support. The research leading to these results has received partial funding from the European Union's Horizon 2020 Programme under grant agreement no. 951774 (FOXES). P.W. further thanks the Alexander von Humboldt Foundation for his postdoctoral fellowship. The authors thank Avantama AG for providing the aluminum-doped zinc oxide nanoparticle dispersion.

■ REFERENCES

(1) Yi, J.; Zhang, G.; Yu, H.; Yan, H. Advantages Challenges and Molecular Design of Different Material Types Used in Organic Solar Cells. *Nat. Rev. Mater.* **2024**, *9* (1), 46−62.

(2) Yan, C.; Barlow, S.; Wang, Z.; Yan, H.; Jen, A. K. Y.; Marder, S. R.; Zhan, X. Non-Fullerene Acceptors for Organic Solar Cells. *Nat. Rev. Mater.* **2018**, *3* (3), 18003.

(3) Krebs, F. C.; Espinosa, N.; Hösel, M.; Søndergaard, R. R.; Jørgensen, M. Anniversary Article: Rise to Power - OPV-Based Solar Parks. *Adv. Mater.* **2014**, *26* (1), 29−39.

(4) Li, G.; Zhu, R.; Yang, Y. Polymer Solar Cells. *Nat. Photonics* **2012**, *6* (3), 153−161.

(5) Cheng, Y. J.; Yang, S. H.; Hsu, C. S. Synthesis of Conjugated Polymers for Organic Solar Cell Applications. *Chem. Rev.* **2009**, *109* (11), 5868−5923.

(6) Mori, S.; Gotanda, T.; Nakano, Y.; Saito, M.; Todori, K.; Hosoya, M. Investigation of the Organic Solar Cell Characteristics for Indoor LED Light Applications. *Jpn. J. Appl. Phys.* **2015**, *54* (7), 071602.

(7) Lee, C.; Lee, J.-H.; Lee, H. H.; Nam, M.; Ko, D.-H. Over 30% Efficient Indoor Organic Photovoltaics Enabled by Morphological Modification Using Two Compatible Non-Fullerene Acceptors. *Adv. Energy Mater.* **2022**, *12* (22), 2200275.

(8) Ma, L. K.; Chen, Y.; Chow, P. C. Y.; Zhang, G.; Huang, J.; Ma, C.; Zhang, J.; Yin, H.; Hong Cheung, A. M.; Wong, K. S.; So, S. K.; Yan, H. High-Efficiency Indoor Organic Photovoltaics with a Band-Aligned Interlayer. *Joule* **2020**, *4* (7), 1486−1500.

(9) Zhang, T.; An, C.; Xu, Y.; Bi, P.; Chen, Z.; Wang, J.; Yang, N.; Yang, Y.; Xu, B.; Yao, H.; Hao, X.; Zhang, S.; Hou, J. A Medium-Bandgap Nonfullerene Acceptor Enabling Organic Photovoltaic Cells with 30% Efficiency under Indoor Artificial Light. *Adv. Mater.* **2022**, *34* (43), 2207009.

(10) Yuan, J.; Zhang, Y.; Zhou, L.; Zhang, G.; Yip, H. L.; Lau, T. K.; Lu, X.; Zhu, C.; Peng, H.; Johnson, P. A.; Leclerc, M.; Cao, Y.; Ulanski, J.; Li, Y.; Zou, Y. Single-Junction Organic Solar Cell with over 15% Efficiency Using Fused-Ring Acceptor with Electron-Deficient Core. *Joule* **2019**, *3* (4), 1140−1151.

(11) Chen, C.; Wang, L.; Xia, W.; Qiu, K.; Guo, C.; Gan, Z.; Zhou, J.; Sun, Y.; Liu, D.; Li, W.; Wang, T. Molecular Interaction Induced Dual Fibrils towards Organic Solar Cells with Certified Efficiency over 20%. *Nat. Commun.* **2024**, *15* (1), 6865.

(12) Wang, J.; Wang, P.; Chen, T.; Zhao, W.; Wang, J.; Lan, B.; Feng, W.; Liu, H.; Liu, Y.; Wan, X.; Long, G.; Kan, B.; Chen, Y. Isomerism Effect of 3D Dimeric Acceptors for Non-Halogenated Solvent-Processed Organic Solar Cells with 20% Efficiency. *Angew. Chem., Int. Ed.* **2025**, *64* (12), e202423562.

(13) Ding, P.; Yang, D.; Yang, S.; Ge, Z. Stability of Organic Solar Cells: Toward Commercial Applications. *Chem. Soc. Rev.* **2024**, *53* (5), 2350−2387.

(14) Zhang, Z. G.; Li, Y. Polymerized Small-Molecule Acceptors for High-Performance All-Polymer Solar Cells. *Angew. Chem., Int. Ed.* **2021**, *60* (9), 4422−4433.

(15) Gasparini, N.; Salleo, A.; McCulloch, I.; Baran, D. The Role of the Third Component in Ternary Organic Solar Cells. *Nat. Rev. Mater.* **2019**, *4* (4), 229−242.
(16) Zhu, Y.; Gadisa, A.; Peng, Z.; Ghasemi, M.; Ye, L.; Xu, Z.; Zhao, S.; Ade, H. Rational Strategy to Stabilize an Unstable High-Efficiency Binary Nonfullerene Organic Solar Cells with a Third Component. *Adv. Energy Mater.* **2019**, *9* (20), 1900376.
(17) Pan, M. A.; Lau, T. K.; Tang, Y.; Wu, Y. C.; Liu, T.; Li, K.; Chen, M. C.; Lu, X.; Ma, W.; Zhan, C. 16.7%-Efficiency Ternary Blended Organic Photovoltaic Cells with PCBM as the Acceptor Additive to Increase the Open-Circuit Voltage and Phase Purity. *J. Mater. Chem. A* **2019**, *7* (36), 20713−20722.
(18) Li, Y.; Huang, X.; Ding, K.; Sheriff, H. K. M., Jr; Ye, L.; Liu, H.; Li, C.-Z.; Ade, H.; Forrest, S. R. Non-Fullerene Acceptor Organic Photovoltaics with Intrinsic Operational Lifetimes over 30 Years. *Nat. Commun.* **2021**, *12* (1), 5419.
(19) Di Mario, L.; Romero, D. G.; Wang, H.; Tekelenburg, E. K.; Meems, S.; Zaharia, T.; Portale, G.; Loi, M. A. Outstanding Fill Factor in Inverted Organic Solar Cells with SnO_2 by Atomic Layer Deposition. *Adv. Mater.* **2024**, *36* (20), 2301404.
(20) Jiang, Y.; Sun, L.; Jiang, F.; Xie, C.; Hu, L.; Dong, X.; Qin, F.; Liu, T.; Hu, L.; Jiang, X.; Zhou, Y. Photocatalytic Effect of ZnO on the Stability of Nonfullerene Acceptors and Its Mitigation by SnO_2 for Nonfullerene Organic Solar Cells. *Mater. Horiz.* **2019**, *6* (7), 1438−1443.
(21) Wang, Y.; Luke, J.; Privitera, A.; Rolland, N.; Labanti, C.; Londi, G.; Lemaur, V.; Toolan, D. T. W.; Sneyd, A. J.; Jeong, S.; Qian, D.; Olivier, Y.; Sorace, L.; Kim, J. S.; Beljonne, D.; Li, Z.; Gillett, A. J. The Critical Role of the Donor Polymer in the Stability of High-Performance Non-Fullerene Acceptor Organic Solar Cells. *Joule* **2023**, *7* (4), 810−829.
(22) Zhang, Q.; Chen, Y.; Liu, X.; Fahlman, M. In Situ Near-Ambient Pressure X-Ray Photoelectron Spectroscopy Reveals the Effects of Water, Oxygen and Light on the Stability of PM6:Y6 Photoactive Layers. *J. Mater. Chem. C* **2023**, *11* (8), 3112−3118.
(23) Jiang, P.; Hu, L.; Sun, L.; Li, Z.; Han, H.; Zhou, Y. On the Interface Reactions and Stability of Nonfullerene Organic Solar Cells. *Chem. Sci.* **2022**, *13* (17), 4714−4739.
(24) Lu, Q.; Yang, Z.; Meng, X.; Yue, Y.; Ahmad, M. A.; Zhang, W.; Zhang, S.; Zhang, Y.; Liu, Z.; Chen, W. A Review on Encapsulation Technology from Organic Light Emitting Diodes to Organic and Perovskite Solar Cells. *Adv. Funct. Mater.* **2021**, *31* (23), 2100151.
(25) Burrows, P. E.; Bulovic, V.; Forrest, S. R.; Sapochak, L. S.; McCarty, D. M.; Thompson, M. E. Reliability and Degradation of Organic Light Emitting Devices. *Appl. Phys. Lett.* **1994**, *65* (23), 2922−2924.
(26) Kovrov, A.; Helgesen, M.; Boeffel, C.; Kröpke, S.; Søndergaard, R. R. Novel Acrylic Monomers for Organic Photovoltaics Encapsulation. *Sol. Energy Mater. Sol. Cells* **2020**, *204*, 110210.
(27) Park, J. S.; Chae, H.; Chung, H. K.; Lee, S. I. Thin Film Encapsulation for Flexible AM-OLED: A Review. *Semicond. Sci. Technol.* **2011**, *26* (3), 034001.
(28) Ahmad, J.; Bazaka, K.; Anderson, L. J.; White, R. D.; Jacob, M. V. Materials and Methods for Encapsulation of OPV: A Review. *Renewable Sustainable Energy Rev.* **2013**, *27*, 104−117.
(29) Carcia, P. F.; McLean, R. S.; Reilly, M.; Groner, M. D.; George, S. M. Ca Test of Al_2O_3 Gas Diffusion Barriers Grown by Atomic Layer Deposition on Polymers. *Appl. Phys. Lett.* **2006**, *89* (3), 031915.
(30) Meyer, J.; Görrn, P.; Bertram, F.; Hamwi, S.; Winkler, T.; Johannes, H. H.; Weimann, T.; Hinze, P.; Riedl, T.; Kowalsky, W. Al_2O_3/ZrO_2 Nanolaminates as Ultrahigh Gas-Diffusion Barriersa Strategy for Reliable Encapsulation of Organic Electronics. *Adv. Mater.* **2009**, *21* (18), 1845−1849.
(31) Meyer, J.; Schmidt, H.; Kowalsky, W.; Riedl, T.; Kahn, A. The Origin of Low Water Vapor Transmission Rates through Al_2O_3/ZrO_2 Nanolaminate Gas-Diffusion Barriers Grown by Atomic Layer Deposition. *Appl. Phys. Lett.* **2010**, *96* (24), 243308.
(32) Behrendt, A.; Friedenberger, C.; Gahlmann, T.; Trost, S.; Becker, T.; Zilberberg, K.; Polywka, A.; Görrn, P.; Riedl, T. Highly Robust Transparent and Conductive Gas Diffusion Barriers Based on Tin Oxide. *Adv. Mater.* **2015**, *27* (39), 5961−5967.
(33) Behrendt, A.; Meyer, J.; Van De Weijer, P.; Gahlmann, T.; Heiderhoff, R.; Riedl, T. Stress Management in Thin-Film Gas-Permeation Barriers. *ACS Appl. Mater. Interfaces* **2016**, *8* (6), 4056−4061.
(34) Brinkmann, K. O.; Becker, T.; Zimmermann, F.; Kreusel, C.; Gahlmann, T.; Theisen, M.; Haeger, T.; Olthof, S.; Tückmantel, C.; Günster, M.; Maschwitz, T.; Göbelsmann, F.; Koch, C.; Hertel, D.; Caprioglio, P.; Peña-Camargo, F.; Perdigón-Toro, L.; Al-Ashouri, A.; Merten, L.; Hinderhofer, A.; Gomell, L.; Zhang, S.; Schreiber, F.; Albrecht, S.; Meerholz, K.; Neher, D.; Stolterfoht, M.; Riedl, T. Perovskite−Organic Tandem Solar Cells with Indium Oxide Interconnect. *Nature* **2022**, *604* (7905), 280−286.
(35) Yu, R.; Yao, H.; Cui, Y.; Hong, L.; He, C.; Hou, J. Improved Charge Transport and Reduced Nonradiative Energy Loss Enable Over 16% Efficiency in Ternary Polymer Solar Cells. *Adv. Mater.* **2019**, *31* (36), 1902302.
(36) Zhao, Y.; Wu, Z.; Liu, X.; Zhong, Z.; Zhu, R.; Yu, J. Revealing the Photo-Degradation Mechanism of PM6:Y6 Based High-Efficiency Organic Solar Cells. *J. Mater. Chem. C* **2021**, *9* (39), 13972−13980.
(37) Groner, M. D.; Fabreguette, F. H.; Elam, J. W.; George, S. M. Low-Temperature Al_2O_3 Atomic Layer Deposition. *Chem. Mater.* **2004**, *16* (4), 639−645.
(38) Classen, A.; Heumueller, T.; Wabra, I.; Gerner, J.; He, Y.; Einsiedler, L.; Li, N.; Matt, G. J.; Osvet, A.; Du, X.; Hirsch, A.; Brabec, C. J. Revealing Hidden UV Instabilities in Organic Solar Cells by Correlating Device and Material Stability. *Adv. Energy Mater.* **2019**, *9* (39), 1902124.
(39) Weitz, P.; orre, V. M. L.; Du, X.; Forberich, K.; Deibel, C.; Brabec, C. J.; Heumüller, T. Revealing Photodegradation Pathways of Organic Solar Cells by Spectrally Resolved Accelerated Lifetime Analysis. *Adv. Energy Mater.* **2023**, *13* (2), 2202564.
(40) Brinkmann, K. O.; Wang, P.; Lang, F.; Li, W.; Guo, X.; Zimmermann, F.; Olthof, S.; Neher, D.; Hou, Y.; Stolterfoht, M.; Wang, T.; Djurišić, A. B.; Riedl, T. Perovskite−Organic Tandem Solar Cells. *Nat. Rev. Mater.* **2024**, *9* (3), 202−217.
(41) Zhao, Y.; Schwab, M. G.; Kiersnowski, A.; Pisula, W.; Baumgarten, M.; Chen, L.; Müllen, K.; Li, C. Trifluoromethyl-Functionalized Bathocuproine for Polymer Solar Cells. *J. Mater. Chem. C* **2016**, *4* (21), 4640−4646.
(42) Brinkmann, K. O.; Zhao, J.; Pourdavoud, N.; Becker, T.; Hu, T.; Olthof, S.; Meerholz, K.; Hoffmann, L.; Gahlmann, T.; Heiderhoff, R.; Oszajca, M. F.; Luechinger, N. A.; Rogalla, D.; Chen, Y.; Cheng, B.; Riedl, T. Suppressed Decomposition of Organometal Halide Perovskites by Impermeable Electron-Extraction Layers in Inverted Solar Cells. *Nat. Commun.* **2017**, *8* (1), 13938.
(43) Hadmojo, W. T.; Isikgor, F. H.; Lin, Y.; Ling, Z.; He, Q.; Faber, H.; Yengel, E.; Ali, R.; Samad, A.; Ardhi, R. E. A.; Jeong, S. Y.; Woo, H. Y.; Schwingenschlögl, U.; Heeney, M.; Anthopoulos, T. D. Stable Organic Solar Cells Enabled by Simultaneous Hole and Electron Interlayer Engineering. *Energy Environ. Mater.* **2024**, *7* (5), e12712.
(44) Dameron, A. A.; Davidson, S. D.; Burton, B. B.; Carcia, P. F.; Mclean, R. S.; George, S. M. Gas Diffusion Barriers on Polymers Using Multilayers Fabricated by Al_2O_3 and Rapid SiO_2 Atomic Layer Deposition. *J. Phys. Chem. C* **2008**, *112* (12), 4573−4580.
(45) Abdulagatov, A. I.; Yan, Y.; Cooper, J. R.; Zhang, Y.; Gibbs, Z. M.; Cavanagh, A. S.; Yang, R. G.; Lee, Y. C.; George, S. M.. A_2O_3 and TiO_2 Atomic Layer Deposition on Copper for Water Corrosion Resistance. *ACS Appl. Mater. Interfaces* **2011**, *3* (12), 4593−4601.
(46) Kim, L. H.; Kim, K.; Park, S.; Jeong, Y. J.; Kim, H.; Chung, D. S.; Kim, S. H.; Park, C. E. Al_2O_3/TiO_2 Nanolaminate Thin Film Encapsulation for Organic Thin Film Transistors via Plasma-Enhanced Atomic Layer Deposition. *ACS Appl. Mater. Interfaces* **2014**, *6* (9), 6731−6738.
(47) Chiu, K.-Y.; Lo, P.-H.; Lin, Y.-R.; Ho, N. K. T.; Liao, Y.-J.; Meng, H.-F.; Chao, Y.-C.; Huang, Y.-Y.; Horng, S.-F.; Zan, H.-W. Stabilized Efficiency of Nonfullerene Organic Solar Cells Under UV-Filtered Sunlight. *Sol. RRL* **2022**, *6* (12), 2200712.

https://doi.org/10.1021/acsami.5c03977
ACS Appl. Mater. Interfaces 2025, 17, 30924−30931

(48) Muñoz-Rojas, D.; Maindron, T.; Esteve, A.; Piallat, F.; Kools, J. C. S.; Decams, J. M. Speeding up the Unique Assets of Atomic Layer Deposition. *Mater. Today Chem.* **2019**, *12*, 96−120.
(49) Levy, D. H.; Freeman, D.; Nelson, S. F.; Cowdery-Corvan, P. J.; Irving, L. M. Stable ZnO Thin Film Transistors by Fast Open Air Atomic Layer Deposition. *Appl. Phys. Lett.* **2008**, *92* (19), 192101.
(50) Hoffmann, L.; Theirich, D.; Pack, S.; Kocak, F.; Schlamm, D.; Hasselmann, T.; Fahl, H.; Raupke, A.; Gargouri, H.; Riedl, T. Gas Diffusion Barriers Prepared by Spatial Atmospheric Pressure Plasma Enhanced ALD. *ACS Appl. Mater. Interfaces* **2017**, *9* (4), 4171−4176.

https://doi.org/10.1021/acsami.5c03977
ACS Appl. Mater. Interfaces 2025, 17, 30924−30931